Journal of Network Intelligence
Taiwan Ubiquitous Information
©2024 ISSN 2414-8105
Volume **9**, Number **2**, May **2024**

Complex Building Laser Measurement Modelling Based on Intelligently Computed 3D Point Cloud Data

Ting Xue*

School of Human Settlements and Civil Engineering
Xi'an Eurasia University, Xi'an 710055, China
Engineering Research Centre of Urban Intelligent Construction
Universities of Shanxi Province, Xi'an 710055, China
13572195349@163.com

Ji-Cai Zou

Second Branch
Shandong High-speed Laigang Lvjian Development Co., Jinan 250100, China
49043244@qq.com

Sharina Huang

Department of Engineering
Krirk University, Bangkhen 10220, Thailand
uv2202@163.com

*Corresponding author: Ting Xue
Received October 18, 2023, revised December 27, 2023, accepted February 7, 2024.

Abstract. *3D laser scanning technology can be used to obtain complete information about large buildings by means of point clouds. In addition, there is no need to contact the measured object during the 3D laser scanning measurement process, so it is possible to obtain building information away from dangerous objects and complex environments. Traditional inspection methods have limitations in terms of efficiency and accuracy, which make it difficult to meet today's needs for inspecting the quality of building walls. Therefore, this work explores the potential of 3D laser scanning technology in complex building measurement modelling through point cloud data and inverse modelling techniques. Firstly, the point cloud slices of the point cloud data acquired by 3D laser scanning are extracted by the RANSAC algorithm. However, the RANSAC algorithm cannot fully identify the noisy points immediately adjacent to the building façade and the computation is time-consuming. Therefore, the Hierarchical Particle Swarm Optimisation (HPSO) algorithm in Intelligent Computing is combined to improve the efficiency and accuracy when extracting point cloud slices. Secondly, a method that can reduce the fitting error of point cloud density to point cloud data is proposed in order to compensate for the shortcomings of 3D laser scanning techniques. Finally, the proposed modelling method is compared with the traditional method of measuring evenness based on ruler, plug ruler and total station. The results show that the proposed modelling method has the characteristics of minimum error and stable error value, and the average value of deviation is only 0.0295 mm, which is highly practical.*
Keywords: 3D laser scanning technology; point cloud data; PSO; data fitting; evenness measurement

1. **Introduction.** Structural inspection modelling of a building usually refers to the collection of data on some of the components and materials of the structure at a specific time, and the use and safety performance of the structure is determined by the corresponding specifications [1,2,3]. Common types of building inspection include verticality inspection of building walls, inclination inspection of buildings, deformation inspection of beams and columns, etc. On this basis, there are also more complex inspection categories such as structural health inspection to judge the structural stress condition and internal damage. From the characteristics of structural inspection, it can be seen that the inspection efficiency in the inspection process often depends on the speed of obtaining building information, the accuracy of obtaining building information and the convenience of manipulation [4,5,6]. Therefore the research direction of structural inspection is developing along the direction of speed, convenience and accuracy.

Building wall evenness is used to describe the degree of unevenness of the wall surface and the overall thinness and thickness of the wall, which is one of the important standards for the acceptance of the quality of building projects [7,8]. Currently, the measurement method of wall evenness mainly relies on simple methods such as ruler and plug ruler, and this detection method will also bring the problems of poor detection accuracy, slow detection speed and low efficiency due to the randomness of selecting detection points [9, 10]. It is also necessary to build scaffolding when inspecting high-rise buildings, which creates a safety hazard for the personal safety of the staff. In the social background of the rapid development of digitalisation, the traditional evenness measurement method is not enough to meet the development needs of wall inspection. Scholars at home and abroad have done research on the application of three-dimensional laser scanning technology in the deformation detection of the measured object, expanding the application field of three-dimensional laser scanning technology, and this mode of three-dimensional laser combined with deformation detection has been widely used [11, 12].

Terrestrial 3D laser scanning inspection method is a new type of building structure inspection method that has gradually emerged in recent years, which is mainly used by terrestrial 3D laser scanner, together with tripod, target ball, target paper, computer and other ancillary accessories. The basic principle is to calculate the time difference between the emitted and received rays and the emission angle to obtain the spatial coordinates of the measurement point, and with the emission of a large number of lasers, the global coordinate information of the building can be obtained. After obtaining all the point cloud data, the required building information can be obtained through the processing of internal data [13].

At present, terrestrial 3D laser scanning technology in the field of tilt and verticality detection has been increasing, due to the terrestrial 3D laser scanning technology through the point cloud data can obtain a wealth of data information, and the wall facade data acquisition is very convenient, greatly reducing the wall verticality and building tilt detection difficulty. Ground-based 3D laser scanning also has an inherent advantage for reverse modelling of buildings because of its global nature. By using terrestrial 3D laser scanning to obtain the global information of the building for reverse modelling, the structural inspection of the building can be carried out efficiently, conveniently and non-destructively due to its non-contact characteristics [14].

However, due to the existence of systematic errors such as point cloud density and point cloud uncertainty in the measurement process, how to reduce the point cloud data errors has become one of the main research directions in this field, which is also the purpose and focus of this work. Based on the above advantages, exploring its application in the field of building inspection has a very broad practical significance and research prospects.

1.1. **Related Work.** 3D laser scanning technology is a new application in the field of measurement. The research of 3D laser scanning technology progressed rapidly in the 1990s, and the results of this technology are now widely used in many industries [15,16]. By the 1990s, the point cloud data acquired by 3D laser scanners have been qualitatively improved in terms of accuracy and efficiency, as well as in terms of point cloud data conversion and processing.

Three-dimensional laser scanning technology is developing rapidly, mapping technology is improving, and technological progress provides technical support for the efficient use of building elevation point clouds to produce building elevation drawings [17]. The external environment, the accuracy of the instrument itself, etc. will affect the accurate acquisition of the target object data by the 3D laser scanner, making the point cloud acquired by scanning noisy, making it difficult to use the subsequent data, and it is necessary to denoise the acquired data before use. In recent years, scholars at home and abroad have proposed some point cloud denoising methods, Xu et al. [18] proposed to segment the building roof point cloud data through the RANSAC algorithm, and increase the improvement of the seed point algorithm, which in turn improves the confidence of the point cloud surface slice segmentation. Meanwhile, the Kd-Tree and R-radius densities are used to optimize the segmented facets, and the point cloud segmentation of building roof facets is effective. Trevor et al. [19] proposed RANSAC combined with the Euclidean clustering algorithm in point cloud segmentation, which improves the accuracy of segmenting point cloud information of the building façade. Burt et al. [20] uses automatic fine segmentation algorithm to process the initial building facade point cloud data, which can accurately segment the building facade point cloud data. In the effect of building facade processing, this algorithm has advantages over RANSAC algorithm. Ma et al. [21] extracted the face slices of the scanned building façade point cloud by the RANSAC algorithm, and added the R radius density algorithm, which further removes the The introduction of R-radius density improves the accuracy of extracted faces, but it cannot completely identify the noise points immediately adjacent to the building façade and the computation is time-consuming.

Wall evenness inspection is a key issue in building quality assessment. The traditional instrument-based wall evenness measurement methods, such as leaning rule, plugging rule, total station, etc., have the problems of complicated operation, accuracy dependent on surveyors, small coverage, no quantitative analysis, lack of digital management, difficult to measure at high places, many safety hazards, no real-time monitoring, and high cost of human resources. On the whole, these traditional measurement methods are limited in efficiency and application, and it is difficult to meet the needs of modern intelligent quality assessment of buildings. The current method is mainly based on image processing and machine learning technology, through the analysis of wall image features to achieve wall defect identification and quality rating, but there are problems such as poor detection stability and weak adaptability to complex environments.

Based on 3D laser scanning technology, Sun et al. [22] explored the influence of mathematical model on building evenness detection, fitted the point cloud data in Geomagic-qualify software, compared the fitted plane with the point cloud, and analysed the evenness of the wall surface. By adding the least square fitting and Huber's iteration method to the wall point cloud data, the best fitting plane can be obtained, which can effectively resist the influence of gross error and improve the accuracy of evenness measurement.

1.2. **Motivation and contribution.** As a typical optimisation algorithm in intelligent computing, Particle Swarm Algorithm (PSO) [23] has a large application in RANSAC algorithm improvement. PSO can find the global optimal model through parallel fast

iteration, effectively identify and exclude outliers, and enable RANSAC to obtain more accurate in-group points [24, 25]. This is more robust and reliable than the random sampling of RANSAC. Meanwhile, PSO is easy to implement parallel computing efficiently on hardware such as GPUs, which can handle large-scale data and significantly reduce the model fitting time of RANSAC. Optimising the search strategy also accelerates the convergence and reduces the time complexity, and the parallel computing performance and global search capability of PSO can significantly compensate for the shortcomings of RANSAC, which is an important means to improve RANSAC. Overall, PSO can simultaneously optimise the accuracy and time performance of RANSAC by improving the fitting efficiency and the ability to identify outliers.

The main innovations and contributions of this work include:

(1) In order to remove the noise immediately adjacent to the building more accurately and quickly, this work proposes a method for denoising the building façade based on the RANSAC algorithm combined with the Hierarchical Particle Swarm Optimisation (HPSO) algorithm [26] in intelligent computing, in order to improve the efficiency of the building denoising and the accuracy of the extracted building façade.

(2) A method that reduces the point cloud density error in the fitting of point cloud data is proposed in order to compensate for the shortcomings of 3D laser scanning techniques. The core idea of the method is the process of discretising the overall point cloud data in chunks and combining them into point cloud area features. The least squares method with singular matrix decomposition was used to fit the wall elevation and generate the point cloud area features.

2. **Inverse modelling based on terrestrial 3D laser scanning technology.**

2.1. **Principles of 3D laser scanning technology.**

A variety of high and new technologies are integrated in the 3D laser scanning system, which enriches the comprehensive performance of the 3D laser scanner. The core of the terrestrial 3D laser scanning system consists of laser ranging system, scanning system and integrated CCD camera. The auxiliary parts include tripod, prism, target, handheld laser rangefinder, power supply, storage, and computer data processing system.

Three-dimensional laser scanning technology is figuratively known as high-definition measurement technology, the basic structural components include laser light source, scanner and so on. Obtaining the point cloud information on the surface of the object is realised by using the emission and reception of the laser, which can measure the reflectivity and the three-dimensional coordinate value of the measured point, and the laser scanning system uses this laser ranging principle to store the point cloud data in the storage device. The complete three-dimensional information of all kinds of entities and real scenes will be collected to the computer equipment, and the data of the measured target will be processed and analysed through the PC data processing software. The composition of the terrestrial three-dimensional laser scanning system is shown in Figure 1.

The principle of laser distance measurement makes use of the characteristics of the laser, calculates the time difference between the laser emission and reception, and combines the speed of the laser to calculate the distance between the laser emission point and the laser reflection point S. Through the goniophotometric system, the horizontal and vertical angles between the laser emission point and the target object can be calculated. By establishing the relationship between the distance and angle between the object to be measured and the laser emission point, the relative position of the object to be measured and the laser emission point $P(x, y, z)$ is determined. The laser emission point is taken as the coordinate origin of the 3D position $P(x, y, z)$ of the DUT; the origin is defined

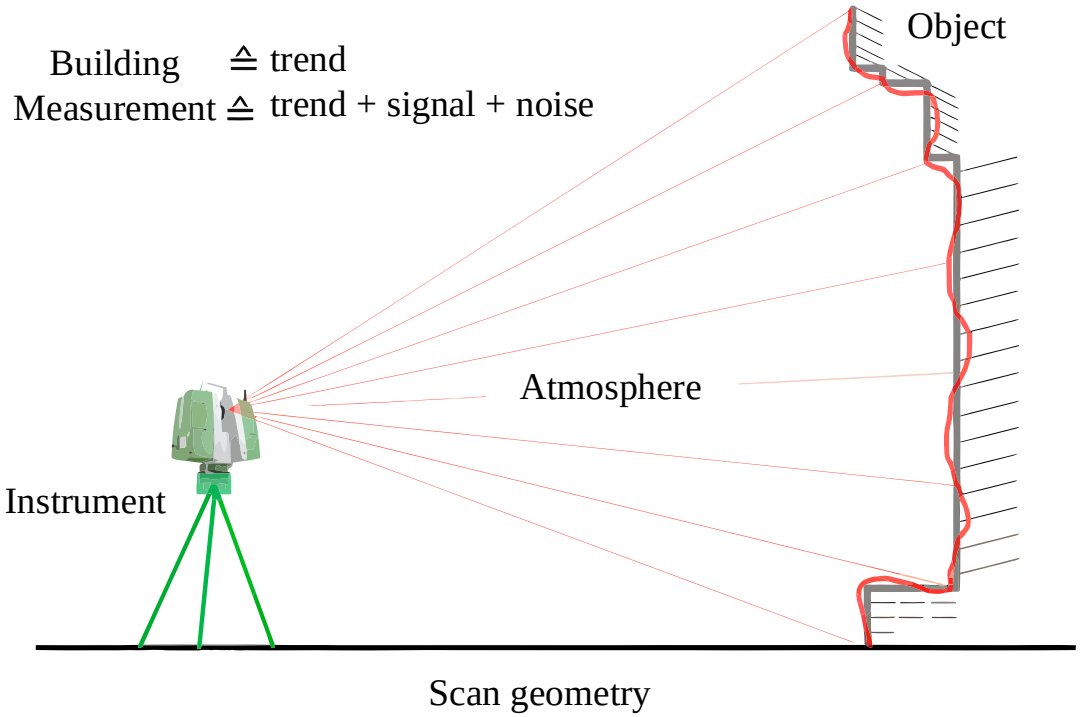

Figure 1. Components of a terrestrial 3D laser scanning system

as the Z-axis vertically and positively upward; in the scanning transverse plane of the instrument, the line perpendicular to the Z-axis from the origin is defined as the X-axis. In the transverse plane of the instrument, the ray from the origin perpendicular to the X-axis and Z-axis at the same time is defined as the Y-axis. The rays point in the direction of the object to be measured as the positive direction of the X-axis and Y-axis. As shown in Figure 2, the origin, X-axis, Y-axis, and Z-axis form a coordinate system, the coordinate system $O - XYZ$ conforms to the right-hand rule.

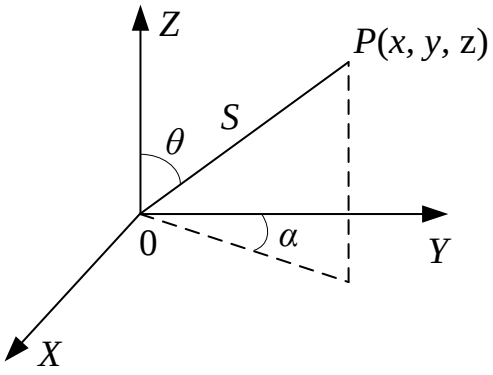

Figure 2. Principles of 3D Coordinate Calculation

The 3D laser scanning system point cloud coordinates are calculated using the formula:

$$\begin{cases} x = S \sin\theta \sin\alpha \\ y = S \sin\theta \cos\alpha \\ z = S \cos\theta \end{cases} \tag{1}$$

The laser beam passes through the same distance once round trip to generate phase difference, the phase method laser distance measurement makes use of this characteristic of the laser beam, by adjusting the amplitude of the continuous laser beam, the phase change generated by the laser beam round trip is calculated, so as to calculate the required time and distance travelled. Ultimately, based on the angle of the scan, combined with the distance between the scanner and the object being measured, the three-dimensional coordinates of the object being measured are calculated.

Phase type laser ranging adjustment container in the middle of the laser round trip, the laser speed is expressed by c, the distance between the laser emission point and the reflection point is expressed by x, the laser emission to receive a round trip time consuming is expressed by t.

$$t = \frac{2x}{c} \tag{2}$$

The frequency of oscillation of a modulating wave is denoted by f and the phase difference between transmission and reception is denoted by φ. The phase difference is given by:

$$\varphi = 2\pi ft = 2\pi N + \Delta\varphi = \frac{4\pi fx}{c} \tag{3}$$

where N denotes the number of complete lower waves of the cycle and $\Delta\varphi$ denotes the residual phase of the wave that is not enough for one cycle.

We can obtain the distance x between the centre position of the scanning instrument and the object to be measured.

$$x = \frac{\varphi c}{4\pi f} = \frac{c}{2f}\frac{(2\pi N + \Delta\varphi)}{2\pi} = \frac{c}{2f}(N + \Delta N) \tag{4}$$

The phase ranging method is used in three-dimensional laser scanning, which is characterised by high ranging accuracy, but the measured distance is relatively short. Generally, within 200 m its measurement accuracy can be up to the millimetre level, so the phase type rangefinder is mainly used in the short and medium distance building measurement.

2.2. **Terrestrial three-dimensional laser scanning equipment.** Terrestrial 3D laser scanning technology in the field of measurement for an emerging technology, in the space three-dimensional acquisition of data has many advantages, breaking through the limitations of the traditional three-dimensional data acquisition and processing of measuring objects. This work uses a Leica ScanStation P50 remote 3D terrestrial laser scanner, as shown in Figure 3. By scanning hard-to-reach locations from a safe position in the field, field time is reduced with fewer setups and productivity is maximised.

The 3D laser scanner acquires the position information of the target and stores it in the form of point cloud coordinates, so the single-point-to-single-point absolute and relative accuracy determines the overall accuracy of the point cloud data. Total stations and 3D laser scanners have the same principles of distance and angle measurement. However, the main errors within the 3D laser scanner system are ranging and angular measurement errors. The nominal error of the measuring instrument is the main factor affecting the ranging and angular errors, and these two errors directly determine the performance of the 3D laser scanner work. The influence of the instrument on the accuracy of the measured point cloud is shown below:

$$m_x^2 = f_{sx}^2 \times m_s^2 + f_{\alpha x}^2 \times m_\alpha^2 + f_{\beta x}^2 \times m_\beta^2 \tag{5}$$

$$m_y^2 = f_{sy}^2 \times m_s^2 + f_{\alpha y}^2 \times m_\alpha^2 + f_{\beta y}^2 \times m_\beta^2 \tag{6}$$

$$m_z^2 = f_{sz}^2 \times m_s^2 + f_{\alpha z}^2 \times m_\alpha^2 + f_{\beta z}^2 \times m_\beta^2 \tag{7}$$

Figure 3. ScanStation P50 remote 3D terrestrial laser scanner

$$\begin{bmatrix} m_x^2 \\ m_y^2 \\ m_z^2 \end{bmatrix} = \begin{bmatrix} f_{sx}^2 & f_{\alpha x}^2 & f_{\beta x}^2 \\ f_{sy}^2 & f_{cy}^2 & f_{\beta y}^2 \\ f_{sz}^2 & f_{oz}^2 & f_{\beta z}^2 \end{bmatrix} \times \begin{bmatrix} m_s^2 \\ m_\alpha^2 \\ m_\beta^2 \end{bmatrix} \tag{8}$$

$$m_p = \sqrt{m_x^2 + m_y^2 + m_z^2} = \sqrt{m_s^2 + \frac{s^2 \times \cos^2\beta}{\rho^2}} \times m_\alpha^2 + \frac{s^2}{\rho^2} \times m_\beta^2 \tag{9}$$

Where m_s is the distance accuracy of the 3D scanner, m_a is the horizontal angular goniometric accuracy of the 3D laser scanner, m_p is the vertical angular goniometric accuracy of the 3D laser scanner, s is the slant distance from the 3D laser scanner to the measured point, and ρ is the adjustment parameter.

In Equation (9) can be seen, the angular and ranging accuracy to determine, analyse the scanner single-point position accuracy shows that: in close observation, its modelled point position positioning accuracy is less than 3mm. three-dimensional laser scanning point accuracy, not only depends on the ranging accuracy is also dependent on the angular accuracy. Angular accuracy on the one hand, we must consider the angle formed by the instrument and the target surface to be measured, the size of the angle will affect the scanning instrument laser reflection signal strength, which in turn affects the instrument measurement error. On the other hand, the angle between the rear view direction and the measured object will also affect the measurement accuracy of the scanning instrument. Experiments show that when the angle between the rear view direction and the measured object is small, the single-point position of the instrument is more accurate, on the contrary, when the angle is large, the single-point position error is larger. In summary, when using 3D laser for physical scanning, we need to choose the appropriate observation distance and observation angle to ensure the accuracy of the measurement point.

3. **RANSAC and HPSO based point cloud facet acquisition.**

3.1. **RANSAC algorithm.** In order to remove the noise immediately adjacent to the building more accurately and quickly, this work proposes a method based on the RANSAC

algorithm combined with the Hierarchical Particle Swarm Optimisation (HPSO) algorithm in Energy Computing for fitting the building façade data, in order to improve the efficiency and accuracy of extracting the building façade.

RANSAC (Random Sampling Consistency) algorithm is an iterative algorithm widely used for model fitting and anti-noise processing. The random sampling method of RANSAC can quickly approximate the optimal model parameters in the sample set containing a large amount of noise, and can effectively resist the interference of the mismatched points, which is suitable for robust fitting and model estimation. According to the idea of RANSAC, as the number of iterations of the algorithm increases, the accuracy of the results obtained is greater. There is a relationship between the probability of ensuring that at least one set of the extracted data is correct.

$$P = 1 - [1 - (1 - \varepsilon)^m]^M \tag{10}$$

Where ε is the probability of error, m is the number of randomly selected data at one time, M is the number of times of cyclic extraction, and P is the confidence level (generally taking the value of 0.9 to 0.99).

Taking the logarithm of Equation (10) gives the number of times required for the loop:

$$M = \frac{\log(1 - P)}{\log(1 - (1 - \varepsilon)^m)} \tag{11}$$

The scanned building elevation point cloud data need to be processed to meet the project use, generally in terms of the building elevation, in the three-dimensional point cloud in the same plane to meet the following relationship:

$$ax + by + cz = d \tag{12}$$

where (x, y, z) are coordinates in 3D space, (a, b, c) are unit plane vectors (the relationship between the three vectors satisfies $a^2 + b^2 + c^2 = 1$), and d is the distance from the origin of the 3D coordinates to the plane.

The parameters of plane equations of different point cloud facets are determined to optimise the original building facade point cloud data. The point cloud acquired by scanning has corresponding 3D coordinates, and the set of m point coordinates is represented by $\{x_i, y_i, z_i\}$. The plane equation expression is shown as follow:

$$[x_i, y_i, z_i, -1]F = 0 \tag{13}$$

$$F = [a, b, c, d]^T \tag{14}$$

The Euclidean distance from the point to the plane S is shown as follow:

$$d_i = |\, ax_i + by_i + cz_i - d \,| \tag{15}$$

Determine the threshold distance δ_0, if the distance d_i is less than δ_0, keep the point as a local point, and vice versa delete the point. Iterate through all the points, you can calculate the number of in-bound points, repeat M times, the plane with the most in-bound points is recorded as S^*, that is, the desired. Finally the points within the S^* plane field (δ_0) are exported and the exported points are used as extracted building facade point cloud data. The schematic diagram of RANSAC point cloud slice extraction is shown in Figure 4.

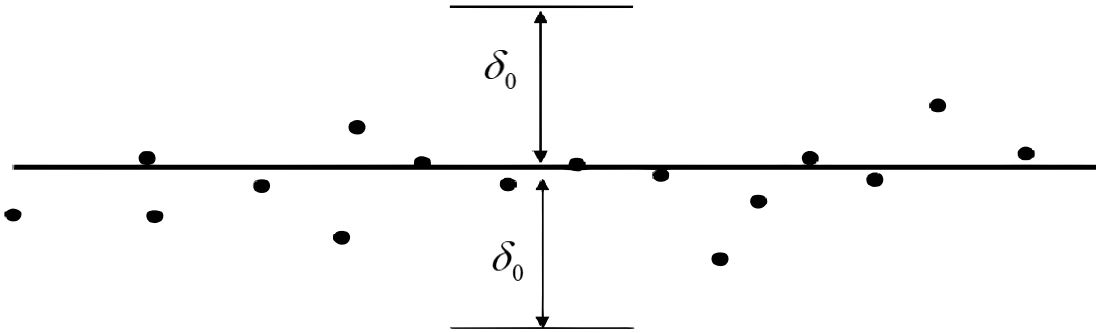

Figure 4. Point cloud facet extraction

3.2. **HPSO algorithm.** In order to remove the noise immediately adjacent to the building more accurately and quickly, the HPSO algorithm is introduced. HPSO is an improved particle swarm optimization algorithm. Its main principle is to divide all particles into multiple levels, and the number of particles in each level follows the pyramid structure, and the number of particles increases gradually from the upper level to the lower level.

The upper particles maintain the overall search direction, and the lower particles converge quickly in a local range. The upper and lower particles exchange information regularly. The upper particles are updated by using the global optimal solution, and the lower particles are updated by using the optimal solution L of this layer, thus realizing the division of labor and cooperation. Through hierarchical division, the interactive range of information is controlled, which not only ensures the global search ability, but also realizes the rapid positioning of the optimal solution. HPSO algorithm makes full use of the idea of multi-particle collaborative optimization and hierarchical control, which makes the search process of complex problems more efficient.

The particle velocity update method is shown below:

$$v_{id}^{k+1} = \omega v_{id}^{k} + c_1 r_1 (p_{id}^{k} - x_{id}^{k}) + c_2 r_2 (p_{gd}^{k} - x_{id}^{k}) \tag{16}$$

$$x_{id}^{k+1} = x_{id}^{k} + r v_{id}^{k+1} \tag{17}$$

where c_1, c_2 are learning factors, ω is the velocity weight of the previous time period, r_1 and r_2 are step parameters.

Firstly, the particles are divided into chunks by space, and the optimal value is solved separately for the particles in each chunk of space, while the position is continuously adjusted according to the global optimal value. The principle of hierarchical particle swarm is described as shown in Figure 5. According to the initial position of the particles, the 160 particles in the particle swarm are divided into 10 groups, each group contains 16 particles. The PSO algorithm is executed in each of the 10 subgroups to update the velocity and position, and each update is compared with the global optimal solution to adjust the direction of the next particle update.

Firstly, the M particle swarms are divided into L parts according to equal amount to establish L subpopulations, Equation (16) and Equation (17) are used to iterate in L subpopulations respectively, as shown in Figure 6. Then the adaptive maxima p_{ig} of the i-th subpopulation is compared with the global maxima p_g, so as to guide the motion direction of the subpopulation particles.

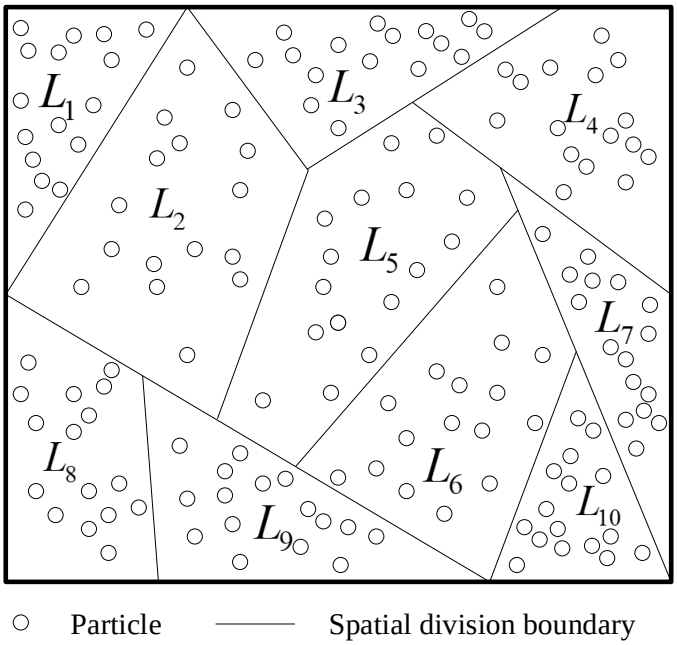

Figure 5. Spatial segmentation of HPSOs

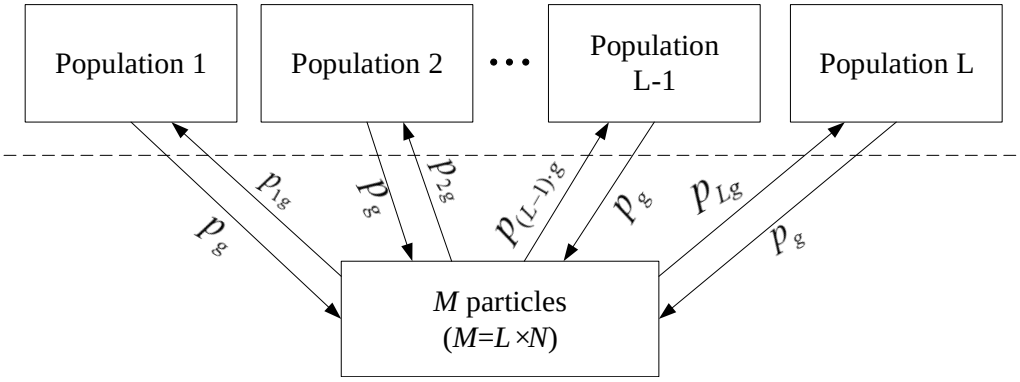

Figure 6. Structure of HPSOs

The subpopulation particles will combine the subpopulation individuals, p_{ig} and p_g, to correct the particle positions. The hierarchical particle swarm velocity update will be improved on the basis of Equation (16) [26].

$$v_{id}^{k+1} = \omega v_{id}^{k} + c_1 r_1 (p_{id}^{k} - x_{id}^{k}) + c_2 r_2 (p_{ig}^{k} - x_{id}^{k}) + c_3 r_3 (p_{g}^{k} - x_{id}^{k}) \tag{18}$$

The c_1, c_2 and c_3 values are set to 2 by default in this work.

4. **Building evenness detection based on point cloud area features.** This work proposes a method that can reduce the point cloud density error on the fitting of point cloud data in order to compensate for the shortcomings of 3D laser scanning techniques. The core idea of the method is the process of discretising the overall point cloud data in chunks and combining them into point cloud area features. The least squares method with singular matrix decomposition was used to fit the wall elevation and generate the point cloud area features [28].

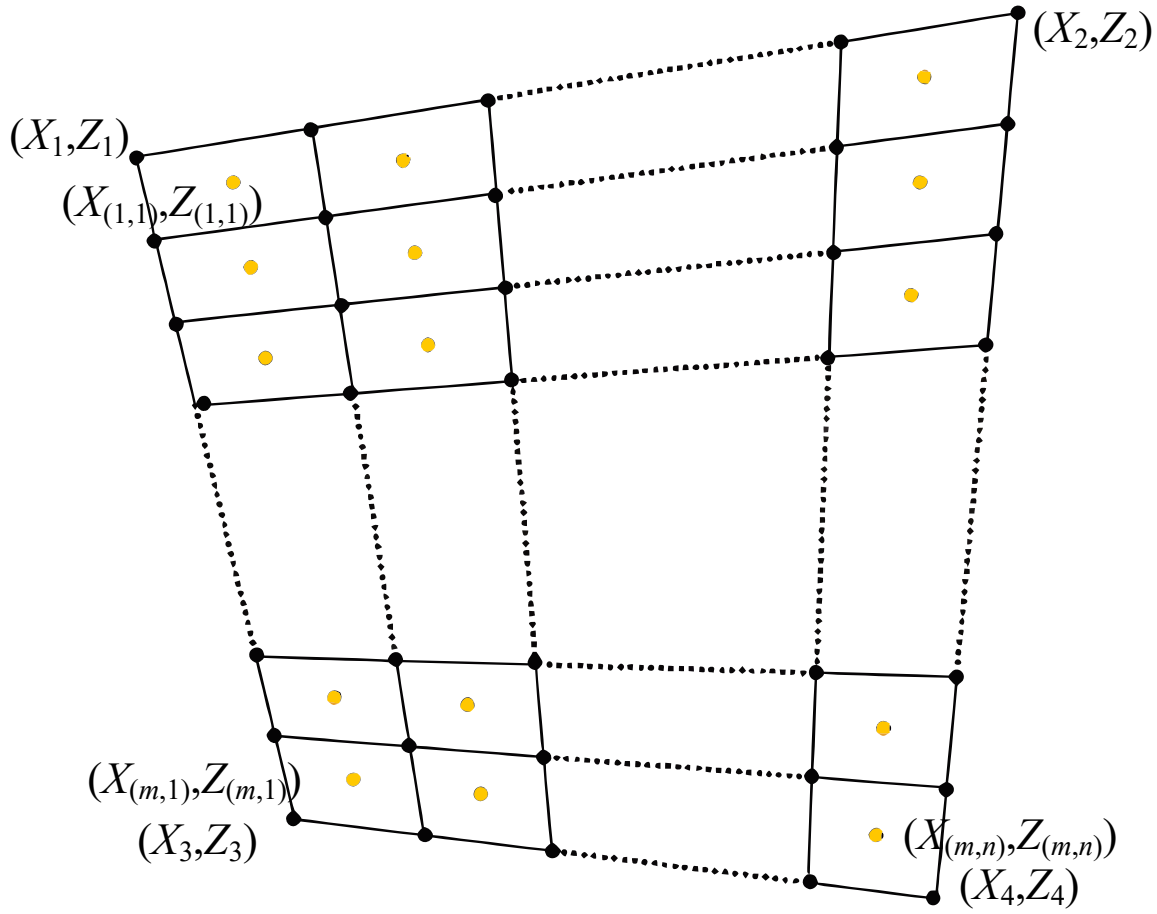

Figure 7. Characterisation of point cloud areas

Through the point cloud processing software, the endpoint coordinate data $A_1(X_1, Y_1, Z_1)$, $A_2(X_2, Y_2, Z_2)$, $A_3(X_3, Y_3, Z_3)$, $A_4(X_4, Y_4, Z_4)$ of this point cloud are obtained. By determining the direction of the plane in which the overall façade is located, the coordinate values of the skeleton points in the plane in which the façade is located are substituted respectively, i.e., the third coordinate value is solved by bringing the two coordinate values into the basic unit plane equation [29]. Assuming that the plane is in the $X - Z$ plane, the point cloud density fluctuates roughly in the Y direction, and the X coordinate values of the corners of the façade are X_1, X_2, X_3 and X_4, as shown in Figure 7.

After obtaining the boundary coordinates, the least squares method can be used to solve for the coordinates of the internal skeleton points, usually the coordinates where the plane is located are derived directly by calculation, and another coordinate value is solved by substituting the obtained coordinates into the equation [30]. When $i \neq 1$, the variation of the X coordinate in the column direction is shown below:

$$\left(X_1 + \frac{(X_2 - X_1)}{n} \times (2j-1)\right) - \left(X_3 + \frac{(X_4 - X_3)}{n} \times (2j-1)\right) / n \times (2i-1) \quad (19)$$

Similarly, for Z-direction coordinates, their variation in the column direction when $i \neq 1$, is shown below:

$$\left(Z_1 + \frac{(Z_2 - Z_1)}{n} \times (2j-1)\right) - \left(Z_3 + \frac{(Z_4 - Z_3)}{n} \times (2j-1)\right) / n \times (2i-1) \quad (20)$$

After obtaining the X and Z coordinates of the point cloud area segmentation points, they are substituted into the basic unit surface equations to obtain the Y coordinates of each basic unit surface, and at the same time, the area segmentation point coordinates are also obtained. After obtaining the area segmentation points, the complete point cloud area characteristics can be obtained by connecting them. By observing the point cloud features, the deformation of the structural façade and the overall change trend can be completely reflected. In the case of wall façade evenness inspection, the point cloud region contained in the façade needs to be fitted numerically.

Due to the small number of segmentation points in the point cloud region, it is easy to use the singular value decomposition method for the operation when fitting the plane through the segmentation points. The point cloud matrix is decomposed as follows:

$$A = U \times S \times V^T \tag{21}$$

where A is the point cloud coordinate matrix, U and V are both correlation unitary matrices, and S is the singular value matrix.

After obtaining the plane equations of the elevations in the point cloud area, the calculation of the evenness can be carried out. The elevation evenness is the offset between the elevation to be measured and the elevation with an angle of 90° to the datum in that direction. According to the angle trigonometric relationship, it can be seen that the relationship of the angle is usually calculated by the value of the cosine of the angle. After obtaining the plane equations, the normal vector is $\mathbf{n} = (A, B, C)$ and the absolute horizontal plane normal phase is $\mathbf{i} = (0, 0, 1)$, then the angle to be measured is calculated as shown as follows:

$$\cos\theta = \cos < \mathbf{n}, \mathbf{i} >= \frac{\mathbf{n} \cdot \mathbf{n}_0}{|\mathbf{n}||\mathbf{n}_0|} \tag{22}$$

Then the evenness offset is:

$$i = H \times \sin(90^\circ - \theta) \tag{23}$$

where H is the height of the elevation to be measured and i is the evenness.

5. Experimental results and analyses.

5.1. Data acquisition.

A ScanStation P50 remote 3D terrestrial laser scanner was used to evaluate the evenness measurements on the east elevation of a building as the measured object. Four measurement points were set up at all four corner points out of the building. The length of the measured object is 81.36 m and the width is 28.13 m. It is necessary to add two measurement stations in the length direction of the measured object to ensure the accuracy of the data in the middle part of the building and the completeness of the acquired data. The measurement points have a wide field of view, and the data between neighbouring measurement points are correlated with each other to form a closed loop.

The acquired point cloud was imported into Scan-Master software [31] for point cloud data stitching processing, and the results are shown in Figure 8. Due to the large volume of the measured object, different stations need to be set up for 3D laser scanning. The coordinate system of different stations is different, and it is necessary to unify the coordinate system of cloud data of different stations. All the point clouds in the basic unit surface are fitted by the least squares method to obtain the basic unit surface equation. After completing the fitting of the basic unit surface equation, the calculation of the coordinates of the pleasing split point can be started.

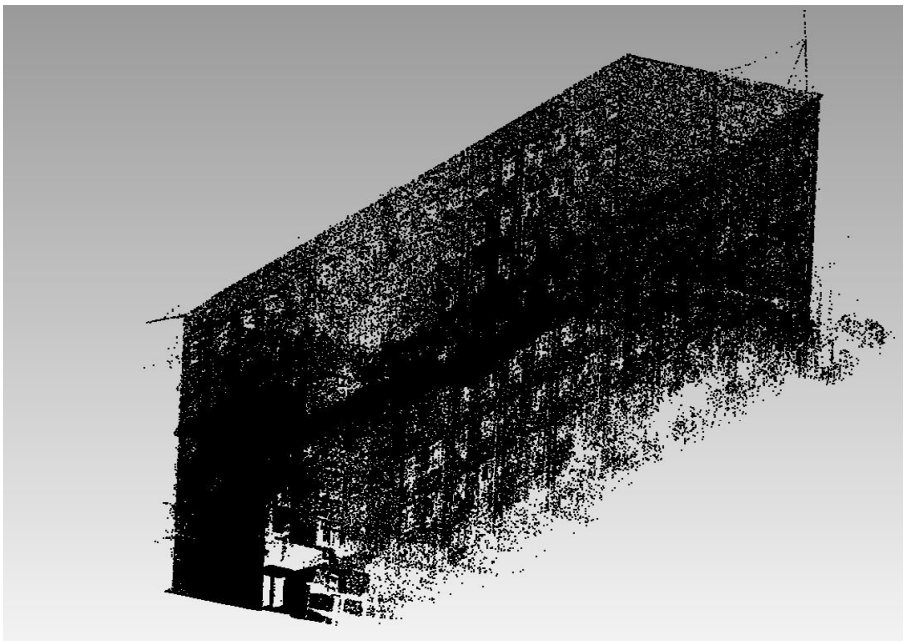

Figure 8. Point cloud of building elevations

5.2. **Optimisation performance of the HPSO algorithm.** The values of the number of subpopulations L and particle velocity weights ω of HPSO affect the convergence speed and global optimisation search performance of the PSO algorithm. In order to verify the optimisation performance of L and ω for point cloud alignment, L and ω are differentially selected to verify the performance of the algorithms proposed in this paper in point cloud data fitting, which is shown in Table 1 and Table 2.

Table 1. Fitting performance of point cloud data with different velocity weights

Speed weight ω	**Rms error**	**Time/s**
0.8	9.211 x 10-5	0.912
0.9	7.142 x 10-5	0.914
1.0	1.802 x 10-5	0.915
1.1	4.873 x 10-6	0.915
1.2	1.091 x 10-5	0.915

From Table 1, it can be seen that the weight increases, the root mean square error of point cloud data fitting shows a trend of decreasing first and then increasing, while the difference in the alignment time is not large; when the weight is 1.1, the feature points of the source point cloud obtained from HPSO search can obtain the optimal matching accuracy after fitting by the RANSAC algorithm.

From Table 2, it can be seen that the root mean square error of the fitted model decreases as the number of subpopulations increases. It can be seen that the higher the number of subpopulations, the more effective the feature point extraction and the higher accuracy of point cloud data fitting. When the number of subpopulations is 6, the root mean square error tends to be stable, with a value of 4.779×10^{-6} . However, as increases, the alignment time also increases gradually, due to the fact that the number of subpopulations is too large causing the extraction of the hierarchical PSO feature points to be more time-consuming. With little difference in time, the number of subgroups is chosen to be 6 which is more suitable for fitting the point cloud data by this method.

Table 2. Performance of point cloud data fitting for number of subgroups

Number of subgroups *L*	**Rms error**	**Time/s**
2	3.717 x 10-5	0.9252
4	7.901 x 10-6	0.9393
6	4.779 x 10-6	0.9416
8	4.762 x 10-6	1.0007
10	4.754 x 10-6	1.0216

5.3. **Comparison of point cloud data fitting performance.** In order to further verify the performance of HPSO+RANSAC in 3D point cloud fitting, the standard RANSAC algorithm and the HPSO+RANSAC algorithm are simulated separately using commonly used Stanford point cloud data samples, and the simulation results are shown in Table 3.

Table 3. Error of fit for different samples

Arithmetic	**Sample point cloud**	**Rms error**
Standard RANSAC	Dragon	5.379 x 10-6
	Han	5.135 x 10-6
	Blade	5.058 x 10-6
	Happy Buddha	5.099 x 10-6
	Horse	5.182 x 10-6
	Bunny	5.059 x 10-6
HPSO+RANSAC	Dragon	5.048 x 10-6
	Hand	4.626 x 10-6
	Blade	3.889 x 10-6
	Happy Buddha	4.279 x 10-6
	Horse	4.409 x 10-6
	Bunny	4.174 x 10-6

It can be seen that compared with the traditional RANSAC algorithm, the HPSO-optimised RANSAC algorithm has a slightly higher fitting accuracy for the six different samples of Stanford's commonly used point cloud databases, but the difference between the two is not significant. The HPSO+RANSAC algorithm has the best alignment performance for the Blade sample, with a RMS error of 3.889×10^{-6}, and the worst for the Dragon sample, with a RMS error of 5.048×10. is the worst, with a root mean square error of 5.048×10^{-6}.

In standard RANSAC, the alignment time is mainly consumed during the iteration process, whereas in the HPSO+RANSAC algorithm, the alignment time is consumed mainly by 2 aspects: feature point extraction and point cloud fitting of the particle swarm. Although the latter increases the feature extraction time, the feature point extraction reduces the number of point clouds in the RANSAC iterations and saves the alignment time.

5.4. **Evenness analysis.** Each of the 30 points on the wall were examined using four evenness detection methods, including lean-to, total station, point cloud, and point cloud area features.

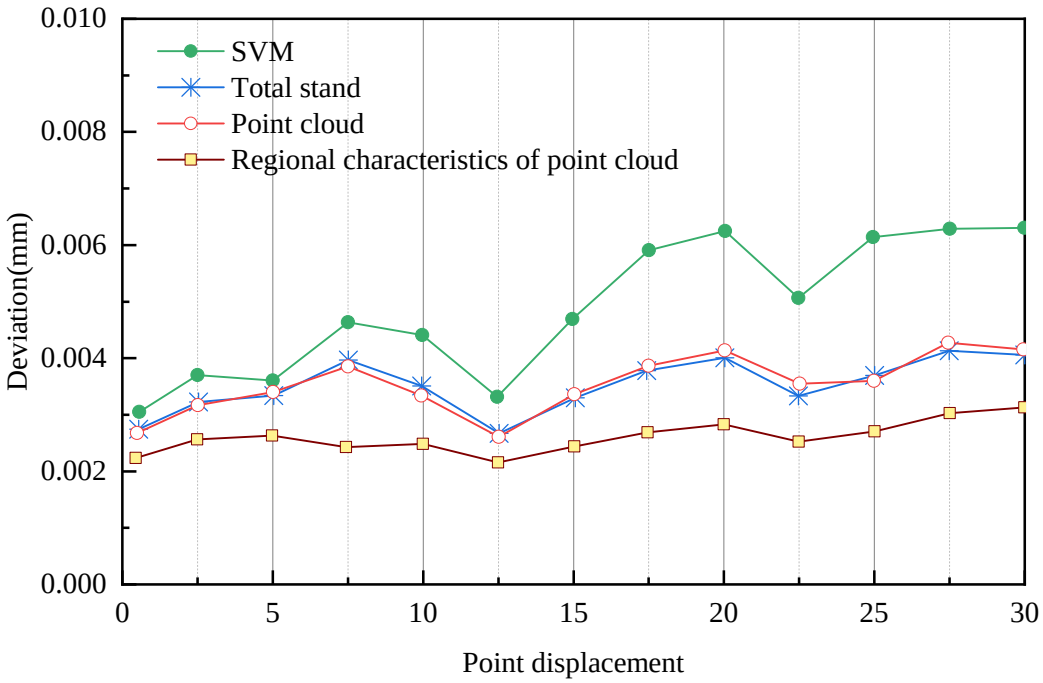

Figure 9. Comparison of bias of different detection methods

The deviation values of the four detection methods are measured for each of the 30 points, and a scatter plot with smoothed lines and data markers is formed with each detection method as a group. As shown in Figure 9, it can be seen that the deviation size of each point position measured by total station and point cloud is similar. Compared with the above two methods, the leaning ruler method has a large reading error and measurement point location error, which can be reduced by averaging the same point over several measurements. In addition, compared with the total station and point cloud, the deviation value of the point cloud area feature is smaller and without big fluctuation, and the average value of the deviation is only 0.0295 mm. Therefore, the building evenness inspection based on the point cloud area feature can be used in the construction inspection of the building project, so as to realize the reliable modelling and to ensure the quality of the construction.

6. **Conclusion.** In this work, the HPSO algorithm in intelligent computing is used for building façade point cloud data fitting to improve the accuracy of point cloud facet extraction. Firstly, a combination of HPSO algorithm and RANSAC is used to improve the efficiency and accuracy of extracting building facades. Secondly, the process of discretising the overall point cloud data in chunks and combining them into point cloud area features. The least squares method with singular matrix decomposition was used to fit the wall façade and generate the point cloud area features. The experimental results show that the HPSO+RANSAC algorithm has high accuracy and efficiency in fitting point cloud data. In addition, the building evenness detection based on the point cloud area features has a small deviation, which enables reliable modelling and ensures construction quality. However, the terrestrial 3D laser scanning technology still has much room for improvement in high-precision measurement and modelling, and future work will try to combine BIM software and 3D laser scanning technology, thus realising the high-precision measurement of entities in building modelling.

Acknowledgment. This work is supported by "The Innovation Team of Eurasia University" of Xi'an Eurasia University (No. 2021XJTD01), and Scientific Research Platform of Eurasia University (No. 2022XJPT01).

REFERENCES

[1] H. Sun, H. V. Burton, and H. Huang, "Machine learning applications for building structural design and performance assessment: State-of-the-art review," *Journal of Building Engineering*, vol. 33, p. 101816, 2021.

[2] D. P. Karuppusamy, "Building detection using two-layered novel convolutional neural networks," *Journal of Soft Computing Paradigm*, vol. 3, no. 1, pp. 29-37, 2021.

[3] B. Bai, W. Fu, T. Lu, and S. Li, "Edge-guided recurrent convolutional neural network for multitemporal remote sensing image building change detection," *IEEE Transactions on Geoscience and Remote Sensing*, vol. 60, pp. 1-13, 2021.

[4] Y. Zhao, T. Li, X. Zhang, and C. Zhang, "Artificial intelligence-based fault detection and diagnosis methods for building energy systems: Advantages, challenges and the future," *Renewable and Sustainable Energy Reviews*, vol. 109, pp. 85-101, 2019.

[5] Y. Liu, C. Pang, Z. Zhan, X. Zhang, and X. Yang, "Building change detection for remote sensing images using a dual-task constrained deep siamese convolutional network model," *IEEE Geoscience and Remote Sensing Letters*, vol. 18, no. 5, pp. 811-815, 2020.

[6] H. Tran, and K. Khoshelham, "Building change detection through comparison of a lidar scan with a building information model," *The International Archives of the Photogrammetry, Remote Sensing and Spatial Information Sciences*, vol. 42, pp. 889-893, 2019.

[7] H. Perez, J. H. Tah, and A. Mosavi, "Deep learning for detecting building defects using convolutional neural networks," *Sensors*, vol. 19, no. 16, p. 3556, 2019.

[8] E. K. Dey, M. Awrangjeb, and B. Stantic, "Outlier detection and robust plane fitting for building roof extraction from LiDAR data," *International Journal of Remote Sensing*, vol. 41, no. 16, pp. 6325-6354, 2020.

[9] H. Perez, and J. H. Tah, "Deep learning smartphone application for real-time detection of defects in buildings," *Structural Control and Health Monitoring*, vol. 28, no. 7, p. e2751, 2021.

[10] W. Cai, X. Wen, S. Wang, and L. Wang, "A real-time detection method of building energy efficiency based on image processing," *Journal of Visual Communication and Image Representation*, vol. 60, pp. 295-304, 2019.

[11] A. L. B. Buck, C. Lingnau, S. Péllico Neto, Á. M. L. Machado, and R. P. Martins-Neto, "Stem modelling of Eucalyptus by terrestrial laser scanning," *Floresta e Ambiente*, vol. 26, p. e20160125, 2019.

[12] T.-Y. Wu, A. Shao, and J.-S. Pan, "CTOA: Toward a Chaotic-Based Tumbleweed Optimization Algorithm," *Mathematics*, vol. 11, no. 10, p. 2339, 2023.

[13] T.-Y. Wu, H. Li, and S.-C. Chu, "CPPE: An Improved Phasmatodea Population Evolution Algorithm with Chaotic Maps," *Mathematics*, vol. 11, no. 9, p. 1977, 2023.

[14] F. Zhang, T.-Y. Wu, Y. Wang, R. Xiong, G. Ding, P. Mei, and L. Liu, "Application of Quantum Genetic Optimization of LVQ Neural Network in Smart City Traffic Network Prediction," *IEEE Access*, vol. 8, pp. 104555-104564, 2020.

[15] L. Kang, R.-S. Chen, N. Xiong, Y.-C. Chen, Y.-X. Hu, and C.-M. Chen, "Selecting Hyper-Parameters of Gaussian Process Regression Based on Non-Inertial Particle Swarm Optimization in Internet of Things," *IEEE Access*, vol. 7, pp. 59504-59513, 2019.

[16] C.-M. Chen, S. Lv, J. Ning, and J. M.-T. Wu, "A Genetic Algorithm for the Waitable Time-Varying Multi-Depot Green Vehicle Routing Problem," *Symmetry*, vol. 15, no. 1, p. 124, 2023.

[17] A. L. H. P. Shaik, M. K. Manoharan, A. K. Pani, R. R. Avala, and C.-M. Chen, "Gaussian Mutation–Spider Monkey Optimization (GM-SMO) Model for Remote Sensing Scene Classification," *Remote Sensing*, vol. 14, no. 24, p. 6279, 22022.

[18] B. Xu, W. Jiang, J. Shan, J. Zhang, and L. Li, "Investigation on the weighted ransac approaches for building roof plane segmentation from lidar point clouds," *Remote Sensing*, vol. 8, no. 1, p. 5, 2015.

[19] A. J. Trevor, S. Gedikli, R. B. Rusu, and H. I. Christensen, "Efficient organized point cloud segmentation with connected components," *Semantic Perception Mapping and Exploration*, vol. 10, no. 6, pp. 251-257, 2013.

[20] A. Burt, M. Disney, and K. Calders, "Extracting individual trees from lidar point clouds using treeseg," *Methods in Ecology and Evolution*, vol. 10, no. 3, pp. 438-445, 2019.

[21] S. Ma, P. Guo, H. You, P. He, G. Li, and H. Li, "An image matching optimization algorithm based on pixel shift clustering RANSAC," *Information Sciences*, vol. 562, pp. 452-474, 2021.
[22] S. Sun, P. He, G. Wang, W. Li, H. Wang, D. Chen, and F. Xu, "Shape characterization methods of irregular cavity using Fourier analysis in tunnel," *Mathematics and Computers in Simulation*, vol. 187, pp. 191-214, 2021.
[23] M. Jain, V. Saihjpal, N. Singh, and S. B. Singh, "An overview of variants and advancements of PSO algorithm," *Applied Sciences*, vol. 12, no. 17, p. 8392, 2022.
[24] A. Pradhan, S. K. Bisoy, and A. Das, "A survey on PSO based meta-heuristic scheduling mechanism in cloud computing environment," *Journal of King Saud University-Computer and Information Sciences*, vol. 34, no. 8, pp. 4888-4901, 2022.
[25] Y. Zhu, G. Li, R. Wang, S. Tang, H. Su, and K. Cao, "Intelligent fault diagnosis of hydraulic piston pump combining improved LeNet-5 and PSO hyperparameter optimization," *Applied Acoustics*, vol. 183, p. 108336, 2021.
[26] H. Tian, H. Fan, M. Feng, R. Cao, and D. Li, "Fault Diagnosis of Rolling Bearing Based on HPSO Algorithm Optimized CNN-LSTM Neural Network," *Sensors*, vol. 23, no. 14, p. 6508, 2023.
[27] V. Ramasamy, and S. Thalavai Pillai, "An effective HPSO-MGA optimization algorithm for dynamic resource allocation in cloud environment," *Cluster Computing*, vol. 23, pp. 1711-1724, 2020.
[28] P. Xiang, X. Wen, Y.-S. Liu, Y.-P. Cao, P. Wan, W. Zheng, and Z. Han, "Snowflake point deconvolution for point cloud completion and generation with skip-transformer," *IEEE Transactions on Pattern Analysis and Machine Intelligence*, vol. 45, no. 5, pp. 6320-6338, 2022.
[29] F. Song, Y. Shao, W. Gao, H. Wang, and T. Li, "Layer-wise geometry aggregation framework for lossless lidar point cloud compression," *IEEE Transactions on Circuits and Systems for Video Technology*, vol. 31, no. 12, pp. 4603-4616, 2021.
[30] Y. Pan, Y. Dong, D. Wang, A. Chen, and Z. Ye, "Three-dimensional reconstruction of structural surface model of heritage bridges using UAV-based photogrammetric point clouds," *Remote Sensing*, vol. 11, no. 10, p. 1204, 2019.
[31] X. Sun, H. Ma, Y. Sun, and M. Liu, "A novel point cloud compression algorithm based on clustering," *IEEE Robotics and Automation Letters*, vol. 4, no. 2, pp. 2132-2139, 2019.